Available online at www.sciencedirect.com

ScienceDirect

Geochimica et Cosmochimica Acta 262 (2019) 207–219

Geochimica et Cosmochimica Acta

www.elsevier.com/locate/gca

Constraints on hydrogen levels in the Archean atmosphere based on detrital magnetite

Shintaro Kadoya *, David C. Catling

Dept. of Earth & Space Sciences, University of Washington, Box 351310, 4000 15th Avenue NE, Seattle, WA 98195-1310, USA

Received 4 December 2018; accepted in revised form 22 July 2019; Available online 2 August 2019

Abstract

The partial pressure of atmospheric hydrogen (pH_2) on the early Earth is important because it has been proposed that high pH_2 warmed the planet or allowed prebiotic chemistry in the early atmosphere. However, such hypotheses lack observational constraints on pH_2. Here, we use the existence of detrital magnetites in ($\sim$ 3.0 Ga) Archean riverbeds to constrain pH_2. Under the condition of high pH_2, magnetite should disappear via reductive dissolution. We investigated the timescale for a magnetite particle in a river to dissolve, which depends on pH_2 and pCO_2. Using published estimates of Archean pCO_2 and assuming the presence of Fe(III)-reducing microbes, the survival timescale is $\sim$ 1 kyr when pH_2 is $\sim 10^{-2}$ bar, and decreases as pH_2 increases. Considering that the residence time of a particle in a short river (< 1000 km) is $\sim$ 1 kyr, the existence of detrital magnetite particles in Archean riverbeds likely indicates that pH_2 was below $\sim 10^{-2}$ bar. Such a level would preclude H_2 as a greenhouse gas or a strongly reducing Archean atmosphere. It is also consistent with limits imposed on H_2 by consumption by methanogens because conversion to CH_4 is thermodynamically favored.

Keywords: Archean; Hydrogen level; magnetite

1. INTRODUCTION

The evolution of atmospheric composition is key for understanding life and habitability on the early Earth. According to stellar evolution theory (e.g., Iben, 1967; Gough, 1981), the early Earth received less insolation from the Sun than today. Large amounts of greenhouse gases would have been necessary to keep the environment warm with such low insolation. While some paleosol analyses indicate that the atmospheric concentration of carbon dioxide (CO_2) was not high enough to keep the surface above the freezing point of water (Rye et al., 1995; Driese et al., 2011), more recent paleosol analyses allow much higher levels of CO_2 (Kanzaki and Murakami, 2015). Possibly, other greenhouse gases, such as methane, may have been necessary (e.g., Haqq-Misra et al., 2008) and would be expected to be abundant in a low oxygen, Archean atmosphere (Catling et al., 2001; Pavlov et al., 2001; Zahnle et al., 2006).

Hydrogen (H_2) is hypothesized to be one of the major gases in the early Earth's atmosphere. Opacity to thermal infrared radiation by collision induced absorption causes H_2 to be a strong greenhouse gas if abundant. Hence, at levels of 10% to 30% of the early atmosphere, hydrogen would have warmed the early Earth (Sagan, 1977; Wordsworth and Pierrehumbert, 2013). Also, H_2 has been proposed as a greenhouse gas on early Mars (Sagan, 1977; Ramirez et al., 2014). In addition, a highly reducing prebiotic atmosphere can give rise to synthesis of prebiotic compounds, such as amino acids (Miller, 1953; Miller and Urey, 1959).

* Corresponding author.
E-mail addresses: skadoya@uw.edu (S. Kadoya), dcatling@uw.edu (D.C. Catling).

https://doi.org/10.1016/j.gca.2019.07.041
0016-7037/

How much H_2 did the early Earth's atmosphere contain? Based on planetary formation theory, the prebiotic atmosphere might have had large amounts of H_2, but H_2 would undergo rapid hydrodynamic escape in the early Hadean (Sekiya et al., 1980). However, it has been suggested that the rate of H_2 escape was throttled because of a lower exobase temperature than present and that the amount of atmospheric H_2 could have been up to ~30% by volume (Tian et al., 2005) although this result is disputed as a numerical artifact of the model that was used (Kuramoto et al., 2013).

Once microbial life arose and diversified, pH_2 for the early Earth would have been lowered by the consumption by methanogens. H_2 ends up in CH_4 when methanogens chemically reduce CO_2 using H_2, producing CH_4. Phylogenetic studies show that methanogens were present by 3.5 Ga and probably much earlier (Wolfe and Fournier, 2018). This is borne out by an occurrence of isotopically light biogenic methane in fluid inclusions in a quartz vein of 3.46 Ga rocks (Ueno et al., 2006). Furthermore, isotopic evidence for ecologically significant microbial methanogenesis is widespread in non-marine settings between 3.0 Ga and 2.7 Ga (Stüeken et al., 2017; Stüeken and Buick, 2018). Assuming that methanogens use the available hydrogen to produce ATP and given the energy that is needed to synthesize 1 mol of ATP, ~ 30 kJ/mol, pH_2 is expected to be no more than $\sim 10^{-4}$ bar (Kharecha et al., 2005; Ozaki et al., 2018).

Thus, previous studies of early Earth's atmospheric pH_2 concentration have approached the problem using theoretical models, but observational constraints are lacking. In this study, we constrain pH_2 using detrital magnetite in Archean riverbeds of age 3.0–2.7 Ga (Srinivasan and Ojakangas, 1986; Donaldson and de Kemp, 1998) described in Section 2.

Ferric ion is far less soluble than ferrous ion, so the dissolution of magnetite ($Fe^{2+}Fe^{3+}_2O_4$) is greatly accelerated by reduction of the ferric iron component. Consequently, the timescale that a magnetite particle lasts would depend on the pH_2 in the environment to reduce the ferric component, so the survival of magnetite particles should set an upper limit on pH_2.

Microbial reduction via Fe(III)-reducing bacteria accelerates the dissolution of magnetite (Schütz et al., 2015). Iron reduction was probably one of the earliest forms of microbial respiration because phylogenetic analysis shows that the most deeply branching microbes near the last common ancestor of extant life can reduce Fe(III) by oxidizing H_2 (Vargas et al., 1998). Additionally, iron isotopes in banded iron formations (BIFs) indicate that microbial reduction was present at ~ 3.1 Ga (Johnson et al., 2008), and might date back to the early Archean (3.7–3.8 Ga; Craddock and Dauphas, 2011; Czaja et al., 2013). Consequently, we assume that such microbes were present by 3.2–2.7 Ga when detrital magnetite is first observed in the geological record. Thus, our main calculations and results include microbial reduction.

We employ a kinetics model to simulate the loss of magnetite by its conversion to other phases and the dissolution of ferrous iron. Using the slowest rate in the range of uncertainty, we estimate an upper limit of the timescale over which magnetite is lost. This upper limit for the timescale provides an upper limit on pH_2 because higher pH_2 would preclude survival of detrital Archean magnetite.

2. REPORTS OF ARCHEAN DETRITAL MAGNETITE

Here, we briefly review the evidence that some magnetite observed in the Archean geologic record was detrital and carried through turbulent rivers that were well mixed with the atmosphere, so that it is valid to use them for pH_2 estimates. As mentioned above, detrital magnetites are reported in Archean fluvial sedimentary rocks in India (Srinivasan and Ojakangas, 1986; Arora, 1991) and Canada (Donaldson and de Kemp, 1998).

The detrital magnetites in India are found in quartzites and quartz-pebble conglomerates in the Bababudan Group in the province of Karnataka in South India. According to U-Pb dating, this unit is now dated at around 2.7 Ga (Trendall et al., 1997).

The Bababudan Group consists of quartz-pebble conglomerates, quartzites, minor metapelites, BIFs, felsic volcanics, and ultramafic rocks. Both the conglomeratic rocks and the quartzites have massive beds, parallel beds, and trough cross-beds. Paleocurrent analysis of cross beds and trough shows low variances of directions, which indicates a fluvial environment. In addition, the volcanic rocks interbedding the quartzites consists of basaltic flows, which are generally amygdaloidal and unpillowed, indicating subaerial deposition. Thus, the quartzites and conglomerates were deposited in a fluvial environment (Srinivasan and Ojakangas, 1986).

The magnetites found here are subrounded to well-rounded. Hence, these minerals are detrital (Srinivasan and Ojakangas, 1986).

In Canada, the detrital magnetites are found in quartz arenite in a 20 m Keeyask Lake sedimentary section in the north western Superior Province. U/Pb dating of detrital zircon gives a depositional age of 2.98 Ga (Donaldson and de Kemp, 1998).

From bottom to top, the Keeyask lake sedimentary section consists of 30 cm thick chert pebble conglomerate, 10 m thick quartz arenite, 15 cm thick columnar and domical stromatolites, and oxide-facies BIF. The bedforms within the quartz arenite comprise planar-stratified beds with symmetrical ripple marks, and cosets of tabular-planar and trough cross-beds including herringbone cross-beds, which indicates that the quartz arenite was deposited during the transition from a continental to shallow-marine environment. The trough crossbeds and symmetrical ripples indicate that the shallow sea water into which rivers flowed was turbulent and well-mixed with the atmosphere.

The quartz arenite bed contains 1% of heavy-minerals by volume, which are mainly pyrite, magnetite, and zircon with lesser amounts of other minerals. Most of the iron oxides are euhedral and authigenic, but some are subrounded grains whose diameter is up to 0.5 mm. Such subrounded grains are interpreted as detrital (Donaldson and de Kemp, 1998).

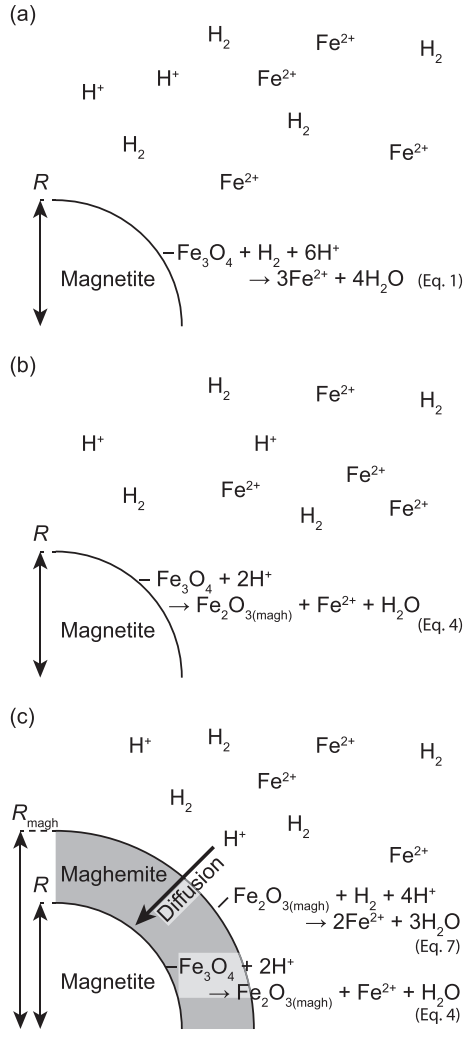

Fig. 1. Model of dissolution of a magnetite particle. When (biotic) reductive dissolution of magnetite is faster than acid dissolution of magnetite, magnetite is directly reduced and releases Fe^{2+} (a); otherwise, acid dissolution of magnetite occurs (b), which might form a maghemite ($Fe_2O_{3(magh)}$) layer (c). While the maghemite layer covers a magnetite core (c), the acid dissolution rate of magnetite follows the supply rate of hydrogen via diffusion through the maghemite layer.

3. MODEL

A model for the dissolution of magnetite is shown schematically in Fig. 1. The overall method is to consider reduction of magnetite by H_2, or at low pH_2, acid-dissolution to make a maghemite layer, which is then reduced. In both cases, Fe^{2+} ions are released into solution. A range of pH is considered from fresh water to siderite-supersaturated. Below, we describe the model.

3.1. Reductive environment

First of all, we consider the case where reductive dissolution of magnetite occurs. The reductive dissolution of magnetite can be written as follows (Sweeton and Baes, 1970; Cornell and Schwertmann, 2003, p.219):

$$Fe_3O_4 + H_2 + 6H^+ \rightarrow 3Fe^{2+} + 4H_2O. \quad (1)$$

According to Kostka and Nealson (1995), a dissolution rate of ferrous ions via biotic reduction of magnetite is 2.45×10^{-5} mol/m^2/h when pH = 5, temperature is 22 °C, and partial pressure of atmospheric hydrogen (pH_2) is 0.1 bar. In addition, the reaction occurs most intensively at pH 5, and both an increase and decrease in pH from pH 5 decrease the dissolution rate (Kostka and Nealson, 1995). Moreover, according to Schütz et al. (2015), the dissolution rate increases with an increase in pH_2.

We also assume that the by-product of biotic reduction does not precipitate on a magnetite particle (Fig. 1a), which is consistent with observations by Schütz et al. (2015). In other words, we assumed (1) that ferrous ions produced by biotic reduction of magnetite immediately dissolve, and (2) that the surface of a magnetite particle always contacts with surrounding water (Fig. 1a).

Hence, the biotic reductive dissolution rate of magnetite (r_{red}) is modeled as follows:

$$\log_{10} r_{red} = \log_{10} k_{red} + \log_{10}\left\{\frac{pH_2}{0.1\ [bar]}\right\} + k_{pH}. \quad (2)$$

Here, we assume that the reductive dissolution rate of magnetite is proportional to pH_2. Also the reference rate (k_{red}) is set at 8.17×10^{-6} mol/m^2/h following Kostka and Nealson (1995). Here, note that since the reductive dissolution of 1 mol of magnetite releases 3 mol of Fe^{2+} (see Eq. 1), the reductive dissolution rate of magnetite is one third of the dissolution rate of ferrous ions (Fe^{2+}). The pH dependence (k_{pH}) is a fit to the results of Kostka and Nealson (1995) as follows:

$$k_{pH} = \begin{cases} 1.132x + 0.2331x^2 & \text{when pH} < 5 \\ -0.5525x + 0.09327x^2 & \text{when pH} > 5 \end{cases}, \quad (3)$$

where x = pH − 5. For the derivation of k_{pH}, see Appendix A. The biotic reductive dissolution rate of magnetite (r_{red}) is summarized in Fig. 2. In Fig. 2, the shrink rate of a mag-

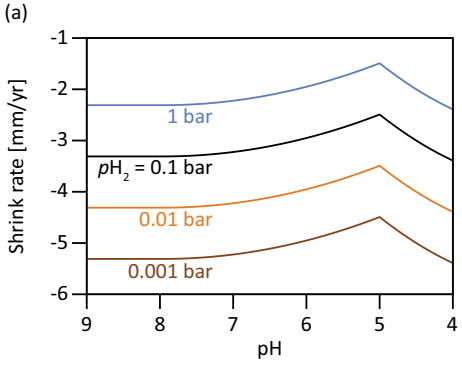

Fig. 2. Shrink rate of a magnetite particle via biotic reductive dissolution for different atmospheric hydrogen levels (pH_2) as a function of pH. The shrink rate is calculated by multiplying a biotic reductive dissolution rate of magnetite (Eq. (2)) and molar volume of magnetite. Biotic reductive dissolution of magnetite occurs most intensively under pH = 5. Both an increase and decrease in pH from pH 5 decreases the dissolution rate (Kostka and Nealson, 1995). In addition, we parameterized how an increase in pH_2 increases the dissolution rate following Schutz et al. (2015).

netite particle (in the unit of [mm/yr]) is calculated by multiplying the dissolution rate, r_{red} [mol/mm^2/yr], by the molar volume of magnetite ($v = 4.5 \times 10^3$ mm^3/mol).

3.2. Less reductive environment

Under a less reducing environment (i.e., magnetite reduction is slow), magnetite abiotically reacts with aqueous hydrogen ions and produces ferrous ion and maghemite (White et al., 1994):

$$Fe_3O_4 + 2H^+ \rightarrow Fe^{2+} + Fe_2O_{3\,maghemite} + H_2O. \quad (4)$$

Maghemite is an isomer of hematite, represented as Fe_2O_3, but can be thought as Fe_2^+-deficient magnetite since it has a magnetite-like cubic crystal structure. Hereafter, this reaction is called "acid dissolution of magnetite".

According to White et al. (1994), the acid dissolution of magnetite is controlled by the supply of H^+ ions, i.e., the pH of the solution. The release rate of ferrous ion, r_{diss} [mol/cm^2/s], is as follows:

$$\log_{10} r_{diss} = \log_{10} k_{mag} - n_{mag} \times pH \quad (5)$$

where $\log_{10} k_{mag}$ [cm^2/s] varies between −12.5 and −13.1 at 25 °C, and n is between 0.21 and 0.29. Hence, when a magnetite particle is in contact with surrounding water, as schematically shown in Fig. 1b, a magnetite particle shrinks, according to r_{diss}.

On the other hand, when a maghemite layer covers a magnetite core (Fig. 1c), the shrink rate of a magnetite core follows a supply rate of hydrogen ion through the magnetite layer. Following the shrinking core model (e.g., Wen, 1968), the shrink rate when it is constrained by the supply of hydrogen ions via diffusion, r_{diff}, can be written as

$$r_{diff} = \frac{D \times 10^{-pH} \times R_{magh}}{2R(R_{magh} - R)}, \quad (6)$$

where R and R_{magh} are a radius of the magnetite core and the maghemite layer. Hence, $R_{magh} - R$ is the thickness of the maghemite layer. In this study, the diffusion coefficient estimated by White et al. (1994) is adopted ($\log_{10} D = -12.2$) where D has units of cm^2/s.

The maghemite produced by acid dissolution of magnetite can also be reduced and dissolve into solution as ferrous ions:

$$Fe_2O_{3\,maghemite} + H_2 + 4H^+ \rightarrow 2Fe^{2+} + 3H_2O. \quad (7)$$

However, the rate of maghemite reduction ($r_{red,magh}$) is unclear. In this study, as a nominal case, we assumed that the Fe^{2+} release rate via maghemite reduction is equal to that of reductive dissolution of magnetite (Eq. (1)). Hence,

$$r_{red,magh} = 1.5 \times r_{mag}. \quad (8)$$

Here, the factor (1.5) is due to the stoichiometry: assuming the same Fe^{2+} release rate, the reduction of maghemite (Fe_2O_3) should be 1.5 times faster than the reductive dissolution of magnetite (Fe_3O_4). Moreover, we also consider two extreme cases of reduction rates in Appendix B as sensitivity tests.

3.3. Numerical procedure

First of all, we compare the biotic reductive dissolution rate of magnetite (r_{red} in Eq. (2)) and acid dissolution rate of magnetite (r_{diss} in Eq. (5)). When $r_{red} > r_{diss}$, we consider that biotic reductive dissolution of magnetite occurs as schematically shown in Fig. 1a. Then, we integrate the following formula:

$$\frac{dR}{dt} = -v r_{red}, \quad (9)$$

where, as before, R is the radius of the magnetite particle in [mm], v is the molar volume of magnetite (4.50×10^4 mm^3/mol), and t is the time in [yr].

On the other hand, when $r_{red} < r_{diss}$, we consider that acid dissolution of magnetite occurs as schematically shown in Fig. 1b and c. Then, we compare the acid dissolution rate of magnetite (r_{diss}) and maghemite reduction rate ($r_{red,magh}$ in Eq. (8)). If $r_{red,magh} > r_{diss}$, maghemite reduction is faster than magnetite dissolution. So, a maghemite layer is not formed as schematically shown in Fig. 1b. Then, we integrate the following formula:

$$\frac{dR}{dt} = -v r_{diss}. \quad (10)$$

Otherwise, maghemite reduction is slower than magnetite dissolution. So, the maghemite layer is formed as schematically shown in Fig. 1c. Then, we integrate the following formulae:

$$\frac{dR}{dt} = -v r_{diff}, \quad \frac{dR_{magh}}{dt} = -v r_{red,magh}, \quad (11)$$

where R_{maghe} is the radius of the maghemite layer in [mm].

We integrate the above formulae from $R = R_0$ to $R = 0$. Here, R_0 is an initial radius of a magnetite particle. When it is necessary to compare R_{magh}, the initial value of R_{magh} is also set at R_0. For all calculations, R_0 is set at 0.25 mm, considering that the largest diameter of observed detrital magnetite particles is 0.5 mm (Donaldson and de Kemp, 1998). We call the time at which the magnetite core disappears (i.e., when $R = 0$) the "survival time".

Table 1 summarizes the parameters applied in this study.

Table 1
Parameters used in this study.

k_{red}	[mol/mm^2/yr]	7.15×10^{-8}	Kostka and Nealson (1995)
k_{mag}	[mol/mm^2/yr]	6.90×10^{-8}	White et al. (1994)
n_{mag}		0.23	White et al. (1994)
$\log_{10} D$	[mm^2/yr]	−2.70	White et al. (1994)
R_0	[mm]	0.25	Donaldson and de Kemp (1998)
v	[mm^3/mol]	4.50×10^4	

3.4. Calculation of pH

We have four cases for the pH calculation: (1) pH as a free parameter, (2) fresh river water in equilibrium with atmospheric CO_2, (3) water saturated with siderite, and (4) water tenfold supersaturated with siderite.

For the first case, we varied pH as a free parameter. For the other cases, we considered the fact that siderite ($FeCO_3$) is not found with the magnetite particles. For the second case, we assume that surrounding water is fresh river water and that hydrogen ions are electronically balanced with carbonate and bicarbonate ions and hydroxide ions. We name this case the "fresh water case". Under this assumption, the following equilibrium states and charge balance for a simple carbonate system are satisfied:

$$\begin{cases} CO_{2(g)} = CO_{2(aq)} \\ CO_{2(aq)} + H_2O = HCO_3^- + H^+ \\ HCO_3^- = CO_3^{2-} + H^+ \\ H_2O = OH^- + H^+ \end{cases} \quad (12)$$

$$[H^+] = [OH^-] + [HCO_3^-] + 2[CO_3^{2-}]. \quad (13)$$

For the third case, we assume that siderite and the surrounding water are in thermodynamic equilibrium. We call this the "siderite saturation case". Under this assumption, the following equilibrium states and charge balance are satisfied in addition to Eq. (12):

$$\begin{cases} FeCO_3 = Fe^{2+} + CO_3^{2-} \\ 2Fe^{2+} + 2H^+ = 2Fe^{3+} + H_2 \\ Fe^{2+} + H_2O = Fe(OH)^+ + H^+ \\ Fe^{3+} + H_2O = Fe(OH)^{2+} + H^+ \end{cases} \quad (14)$$

$$[H^+] + 2[Fe^{2+}] + 3[Fe^{3+}] + [Fe(OH)^+] + 2[Fe(OH)^{2+}] = [OH^-] + [HCO_3^-] + 2[CO_3^{2-}]. \quad (15)$$

Siderite does not always precipitate even under the siderite saturation. According to Postma (1981), siderite precipitates when the saturation state of siderite is ~ 10. Hence, for the fourth case, we assume the supersaturation of siderite. Under this assumption, pH is calculated in the same manner of the siderite saturation case. However, the saturation state of siderite is set at 10.

4. RESULTS

Fig. 3 shows the biotic survival time as a function of pH and pH_2. The dashed gray line in Fig. 3 represents the pH_2 at which the biotic reductive dissolution rate of magnetite (r_{red} in Eq. (2)) is equal to the acid dissolution rate of magnetite (r_{diss} in Eq. (5)). When pH_2 is higher than the dashed gray line, r_{red} is higher than r_{diss}, so biotic reductive dissolution of magnetite occurs as shown in Fig. 1a. On the other hand, when pH_2 is lower than the dashed gray line, r_{diss} is higher than r_{red}, so magnetite dissolution occurs as shown in Fig. 1b and c.

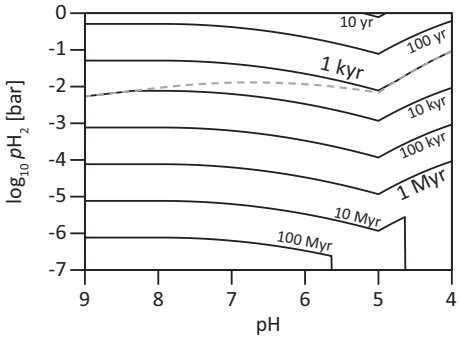

Fig. 3. Biotic survival time of a magnetite particle with initial radius of 0.25 mm as a function of pH and pH_2. The dashed gray line represents the condition where a biotic reductive dissolution rate of magnetite is equal to the acid dissolution rate of magnetite. When pH_2 is higher than this line, biotic reductive dissolution of magnetite occurs; otherwise, acid dissolution of magnetite occurs (i.e., maghemite is formed) before reductive dissolution of maghemite.

When biotic reductive dissolution occurs (i.e., above the dashed gray line in Fig. 3), the survival time is calculated by the integration of Eq. (9):

$$t_{red} = \frac{R_0}{v r_{red}}. \quad (16)$$

Thus, the survival time of this case (hereafter, named as a "magnetite reduction time") is proportional to the inverse of r_{red}, which, in turn, depends on pH_2 (Eq. (2)). Hence, the magnetite reduction time decreases with an increase in pH_2 (Fig. 3; see also Fig. 2). In addition, assuming the same pH_2 condition, the magnetite reduction time is shorter at pH = 5 than at other pH values (Fig. 3; see also Fig. 2).

On the other hand, when magnetite dissolution occurs (i.e., below the dashed gray line in Fig. 3), the survival time is calculated by the integration of Eqs. (10) and (11). As shown in Fig. 3, even under the magnetite acid dissolution case, the survival time tends to decrease with an increase in pH_2 and tends to be shorter at pH = 5 than other pH condition, which is similar to the case of the biotic reductive dissolution (i.e., above the dashed gray line). This is because the survival time is controlled by the biotic maghemite reduction rate. For a nominal case, we assumed that the biotic maghemite reduction rate scales as $r_{red,magh} = 1.5 r_{red}$ from the stoichiometry in Eq. (8).

However, in the lower right of Fig. 3 (i.e., under low pH and low pH_2), the survival time is controlled by the acid dissolution of magnetite and limited by the H^+ supply via diffusion. This is represented by the vertical contour lines. The survival time for this case can be calculated as

$$\log_{10} t_{diff} = 2\log_{10} R_0 - \log_{10} v - \log_{10} D + pH - \log_{10} 3. \quad (17)$$

Hereafter, we name this survival time as a "diffusion time".

The survival time for a less reductive environment strongly depends on the maghemite reduction rate, especially if $pH_2 <\sim 10^{-2}$ bar (see Appendix B). However, when pH > 5, the survival time is at least longer than one thousand years.

5. DISCUSSION

5.1. Condition where biotic magnetite reduction can occur

In this study, we assume that detrital magnetite is biotically reduced with H_2 and that the product of this reaction (i.e., Fe^{2+}) goes into solution. Thus, we model that a reductive dissolution rate of magnetite depends on pH_2 and pH. However, first, the dissolution rate of Fe^{2+} should also depend on a concentration of Fe^{2+} ($[Fe^{2+}]$) itself. Second, if $[Fe^{2+}]$ was high, $Fe(OH)_2$ (Fe-brucite) might precipitate (Tosca et al., 2018) and coat a magnetite particle, preventing further reduction of magnetite. Third, since we assume that microbes derive energy for metabolism via Fe(III)-reduction, the biotic reduction could be affected by the $[Fe^{2+}]$. We consider these three possible complications and show they are not important for our main result.

First, we consider the possibility of $Fe(OH)_2$ precipitation. When a reduction of magnetite produces $Fe(OH)_2$, this reaction can be written as:

$$Fe_3O_4(s) + H_2(g) + 2H_2O(l) \rightarrow 3Fe(OH)_2(s). \quad (18)$$

The change of Gibbs free energy via this reaction ($\Delta G^0 \equiv \sum G^0_{products} - \sum G^0_{reactants}$) is +11.54 kJ/mol at 25 °C, which corresponds to $K_{eq} \sim 10^{-2.0}$ (where K_{eq} is an equilibrium constant). Since $K_{eq} \approx 1/pH_2$, precipitation of Fe$(OH)_2$ is not favored when $pH_2 <\sim 100$ bar. Note that thermodynamic properties are from SLOP16.[1] Hence, precipitation of $Fe(OH)_2$, which prevents reduction of magnetite, can be neglected.

Second, we consider the effect of saturation of ferrous ion (Fe^{2+}). As explained above, we assume that reductive dissolution of magnetite is written as

$$Fe_3O_4 + H_2 + 6H^+ \rightarrow 3Fe^{2+} + 4H_2O. \quad (19)$$

The empirical minimum energy necessary for metabolic production of ATP via a reaction (ΔQ_{met}) is ~ 20 kJ/mol (e.g., Schink, 1997), so the energy yielded by the reaction in Eq. (19) should be larger than ~ 20 kJ/mol. Solid black lines in Fig. 4 represents a concentration of ferrous ion ($[Fe^{2+}]$) under which the energy released by this reaction is 20 kJ/mol. When $[Fe^{2+}]$ is lower than this line, the biotic reductive dissolution of magnetite would be able to occur following the reduction rate assumed in this study.

On the other hand, detrital magnetite particles do not co-exist with siderite (Srinivasan and Ojakangas, 1986; Donaldson and de Kemp, 1998). Hence, we can assume that siderite ($FeCO_3$) was not saturated. A dashed line in Fig. 4 represents a concentration of Fe^{2+} where siderite is saturated (i.e., $Fe^{2+} + CO_2 + H_2 = FeCO_3 + 2H^+$). Accordingly, the absence of siderite would indicate that $[Fe^{2+}]$ was lower than the dashed line in Fig. 4a.

The pH of surface waters depends on partial pressure of atmospheric CO_2 (pCO_2). The pCO_2 range is 5×10^{-3} bar to 0.2 bar at 3.0 Ga assuming 1% of atmospheric CH_4 (Krissansen-Totton et al., 2018). Hence, the corresponding pH range is between 5.7 and 6.8. Here, we assume the siderite saturation case for the pH calculation. Therefore, the ferrous ion indicated by the absence of siderite and pCO_2 range is shown by the gray shaded region in Fig. 4a.

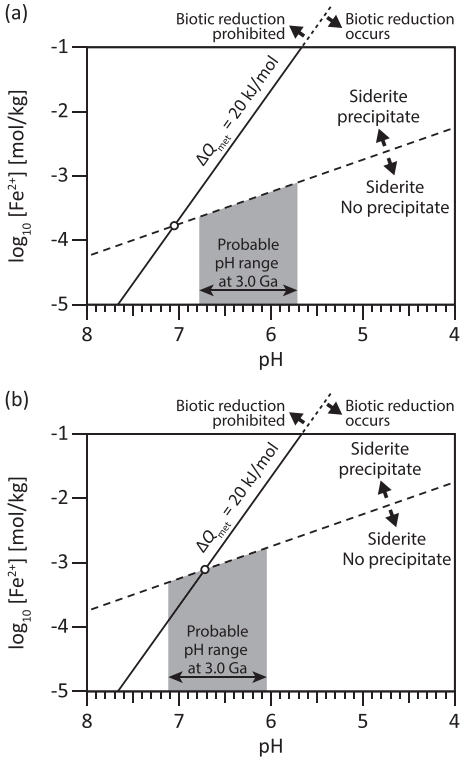

Fig. 4. Concentration of ferrous ion ($[Fe^{2+}]$) as a function of pH. These figures shows the pH condition where biotic reductive dissolution of magnetite occurs according to the $[Fe^{2+}]$ value. The partial pressure of atmospheric hydrogen is set at 0.01 bar. For (a), siderite saturation is assumed; and for (b), siderite tenfold supersaturation is assumed. Dashed lines represent a threshold of $[Fe^{2+}]$ at which siderite precipitates. Solid lines represent a maximum $[Fe^{2+}]$ and maximum pH under which biotic reduction can occur with an assumption of minimum energy necessary for biotic metabolic activity (ΔQ_{met}). Small circles represent the point at which the dashed line intersects with the solid line: for (a), the circle is at pH 7.1, and for (b), it is at pH 6.7. To the right of the white circle, the dashed line is below the solid line, so the absence of siderite (Donaldson and de Kemp, 1998, e.g.,) ensures the biotic reduction of magnetite if pH is lower than the value corresponding to the white circle. Considering the pCO_2 range at 3.0 Ga (i.e., 5×10^{-3} bar to 0.2 bar) that is estimated by Krissansen-Totton et al. (2018) (the corresponding area is indicated by gray shaded region), the corresponding pH range is lower than the maximum pH (i.e., pH 7.1) for (a), but the range contains the maximum pH (i.e., pH 6.7) for (b).

As shown in Fig. 4a, the $[Fe^{2+}]$ value indicated by the absence of siderite and the pCO_2-related pH range (i.e., the gray shaded region) is far below the solid black line (i.e., the maximum $[Fe^{2+}]$ values and maximum pH for biotic reduction). For example, when pH = 6.8 (i.e., $pCO_2 = 5 \times 10^{-3}$ bar), the maximum $[Fe^{2+}]$ indicated by the absence of siderite is 2.31×10^{-4} mol/kg (the dashed line in Fig. 4), which is ~ 2.6 times lower than the saturation level of $[Fe^{2+}]$ assuming $\Delta Q_{met} = 20$ kJ/mol (the solid black line in Fig. 4). Similarly, when pH = 5.7 (i.e.,

[1] doi: https://doi.org/10.5281/zenodo.2630820.

$pCO_2 = 0.2$ bar), the maximum $[Fe^{2+}]$ indicated by the absence of siderite is 7.9×10^{-4} mol/kg, which is roughly 100 times lower than the saturation level of $[Fe^{2+}]$. Therefore, considering the absence of siderite and plausible range of pCO_2, the saturation of ferrous ion should not affect the reaction rate, and therefore the results.

In the above, we assumed that 1% atmospheric methane in the Archean. If there was not atmospheric methane, pCO_2 would be higher and pH would be lower to warm the early Earth (Krissansen-Totton et al., 2018). A decrease in pH increases the difference between concentrations of ferrous ion of saturation level and that indicated by the absence of siderite (Fig. 4). Hence, the absence of atmospheric methane does not change the conclusion that saturation of Fe^{2+} should not affect the reaction rate.

The minimum energy via a reaction might be lower than 20 kJ/mol. For example, a methanogen seems to maintain a condition where an energy yield is 10 kJ/molCH_4 (Hoehler et al., 2002). Moreover, Jackson and McInerney (2002) reported fermentative bacteria that grows even under a condition where a free energy change is 4.5 kJ/mol. If the threshold energy for Fe(III)-reducing bacteria was lower than 20 kJ/mol, the saturation level of $[Fe^{2+}]$ would be higher than that of $\Delta Q_{met} = 20$ kJ/mol; therefore, the absence of siderite would indicate more undersaturation of Fe^{2+}.

For the siderite (tenfold) supersaturation case, the $[Fe^{2+}]$ indicated by the absence of siderite is higher than for the siderite saturation case (solid black line in Fig. 4b). In addition, the pH range for the siderite supersaturation case is also higher than that for the siderite saturation case owing to the abundant ferrous ions (gray shaded regions in Fig. 4b). Accordingly, the black solid line (the maximum pH and maximum $[Fe^{2+}]$ for biotic reduction) crosses the gray shaded region (plausible range for $[Fe^{2+}]$) between pH 6.7 and pH 7.1. The pH > 6.7 corresponds to $pCO_2 < 2.0 \times 10^{-2}$ bar, and the probability of $pCO_2 < 2.0 \times 10^{-2}$ bar is 26% according to Krissansen-Totton et al. (2018) (see also Fig. C.1). Hence, the possibility that the biotic reduction is prohibited is moderate. This point will be discussed later.

If the $[Fe^{2+}]$ is too high, then the energy release from biotic magnetite reduction can be less than ΔQ_{met}. In this case, the flux of Fe^{2+} transported by river water could limit the biotic reductive dissolution rate of magnetite. Also, if the transport of Fe^{2+} is extremely slow, the biotic reductive dissolution rate of magnetite becomes that of the abiotic reaction.

5.2. Constraint on atmospheric hydrogen levels

Detrital magnetite particles found in the Keeyask Lake sedimentary assemblage of the Superior Province of Canada are subrounded grains up to 0.5 mm in diameter, which are in a deposit from a continental to shallow-marine environment from approximately 3.0 Ga (Section 2). Moreover, considering the geological context, particles were in water that was mixed well with the atmosphere. In addition, these particles traveled in a river because they coexist with quartz arenite. Hence, we can apply the assumption of fresh water and/or siderite (super) saturation for the particles in the Keeyask lake even though they ended up deposited in the shallow-marine environment. Besides, we can assume that the particles had been in the water which was mixed well with the atmosphere.

As explained above, a magnetite particle with a radius of 0.25 mm dissolves in tens of years to hundreds of millions of years with the timescale mainly depending on pH_2 (Fig. 3). It is instructive to compare the calculated survival timescale with the time that detrital particles spend in rivers. According to Johnson et al. (2014), the residence time of a particle in a river is 1 kyr to 10 kyr for short river systems (< 1000 km) and 100 kyr to 500 kyr for long river systems (> 1000 km).

Consider the case that a magnetite particle flowed in a short river system with a residence time (t_{res}) of 1 kyr. We can calculate the distribution of survival time given a value of pH_2 using the survival time as a function of pH_2 and pCO_2 (i.e., Fig. 5) and the distribution of pCO_2 at 3.0 Ga. The distribution of pCO_2 follows Krissansen-Totton et al. (2018) (see also Fig. C.1). If $pH_2 > 4.6 \times 10^{-2}$ bar, the probability, $P(t_{surv} > 1\ \text{kyr})$, is lower than 5% (Table 2; see also Fig. 5). Hence, a magnetite particle would probably disappear in a short river system if $pH_2 > 4.6 \times 10^{-2}$bar. Therefore, to explain the existence of detrital magnetite particles, pH_2 was below 4.6×10^{-2} bar.

Similar calculations were done for the siderite saturation case (Fig. 5) and supersaturation case (Fig. 5c). However, as explained in Section 5.1, the limitation of biotic reduction by Fe^{2+} saturation should be considered.

In Fig. 5b and c, dotted black lines represent the maximum pH and minimum pCO_2 limit for biotic reduction. Here, the minimum pCO_2 (maximum pH) limit for biotic reduction corresponds to the condition under which the maximum $[Fe^{2+}]$ allowing biotic reduction is equal to the maximum $[Fe^{2+}]$ indicated by the absence of siderite. The maximum $[Fe^{2+}]$ is calculated assuming the minimum energy for metabolism is 20 kJ/mol (Schink, 1997). Namely, the minimum pCO_2 limit (i.e., the maximum pH limit) for biotic reduction corresponds to the small circle in Fig. 4, where the solid black line (the maximum $[Fe^{2+}]$ for biotic reduction) and dashed line (the maximum $[Fe^{2+}]$ indicated by the absence of siderite) intersect with each other. Hence, biotic reduction of magnetite can occur if pH is lower than the maximum pH for biotic reduction (i.e., pCO_2 is higher than the dotted black line in Fig. 5 to make pH low). Otherwise, biotic reduction would be prohibited, and the magnetite reduction rate would be limited by Fe^{2+} transportation by the river water. Hence, the rate would be slower than the rate assumed in this study. Accordingly, the survival time to the left of the dotted black line in Fig. 5b and c is a minimum estimate because the calculation does not include water transport of Fe^{2+}.

To estimate a conservative upper limit on pH_2, we assume that the survival time is larger than the assumed residence time of a particle in a river (i.e., 1 kyr) under conditions where biotic reduction is prohibited. Then, for the siderite precipitation case (Fig. 5b), the upper limit of pH_2 is 3.7×10^{-2} bar (Table 2). For the siderite supersaturation case (Fig. 5c), the upper limit of pH_2 is 2.9×10^{-1} bar (Table 2).

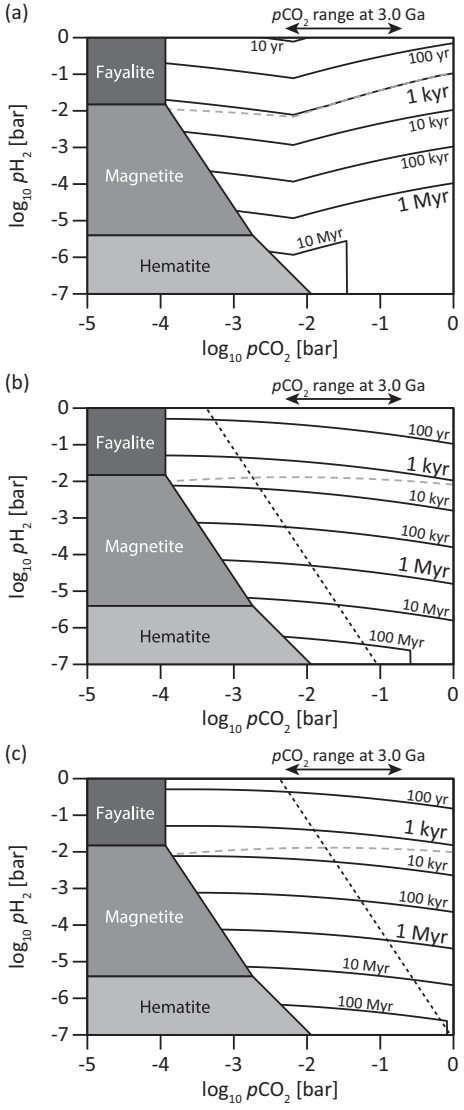

Fig. 5. Biotic survival time of a magnetite particle with initial radius of 0.25 mm. The horizontal axis is pCO_2, and the vertical axis is pH_2 in all diagrams. The difference among panels (a), (b), and (c) is how we calculate pH. For (a), fresh water is assumed. For (b), siderite saturation is assumed. For (c), siderite supersaturation is assumed. Double-sided arrows represent a pCO_2 range at 3.0 Ga assuming 1% CH_4 (Krissansen-Totton et al., 2018). On the other hand, dotted black lines in panels (b) and (c) represent a threshold for biotic reductive dissolution of magnetite. When pCO_2 (or pH_2) is lower than the threshold, the biotic reductive dissolution of magnetite would be limited by transport of ferrous ion. Hence, under such a condition (i.e., left of the dotted black line), the survival time would be longer than the value estimated here.

In the above, we assumed that the atmosphere contains 1% of CH_4. However, even if we apply an assumption that the atmosphere does not contain CH_4, the threshold pH_2 does not change much and is on the order of 10^{-2} bar: for the fresh water case, the threshold pH_2 is 7.7×10^{-2} bar; for the siderite saturation case, 3.2×10^{-2} bar; and for the siderite supersaturation case, 3.8×10^{-2} bar (Table 2).

Table 2
Threshold values of pH_2. When pH_2 is higher than these values, magnetite should have disappeared. Thus, to explain detrital magnetite particles, pH_2 should have been lower than these values. The survival time (t_{surv}) is compared with the residence time of a particle in a short river system (=1 kyr) to derive these pH_2 values.

	pH_2 [bar]
with 1% CH_4	
Fresh water	4.6×10^{-2}
Siderite saturation	3.7×10^{-2}
Siderite supersaturation	2.9×10^{-1}
without CH_4	
Fresh water	7.7×10^{-2}
Siderite saturation	3.2×10^{-2}
Siderite supersaturation	3.8×10^{-2}

5.3. Effect of saturation state

As explained above, the constraint on pH_2 based on the existence of magnetite particles is 3.7×10^{-2} bar if we assume siderite precipitates at a saturation state of unity. On the other hand, the constraint is 2.9×10^{-1} bar when siderite precipitates at a saturation state of ten (Table 2). Thus, the constraint on pH_2 increases with an increase in threshold saturation state of siderite (hereafter, the threshold saturation sate of siderite is written as Ω_{sid}). However, as shown in Fig. 6, the dependence on Ω_{sid} of pH_2 constraint is relatively small for $\log_{10}\Omega_{sid} < 0.5$. So, it is beneficial for pH_2 constraint to estimate the range of Ω_{sid}.

According to Postma (1981), Ω_{sid} increases with an increase in pH; for example, when $pH = \sim 6.4, \Omega_{sid}$ is 1, and when $pH = \sim 7.6, \Omega_{sid}$ is 10. On the other hand, as

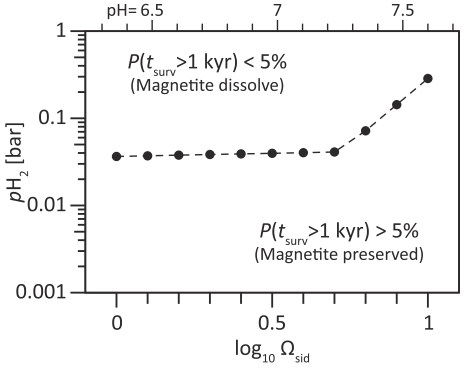

Fig. 6. Upper limit of pH_2 as a function of saturation state of siderite at which siderite precipitates (Ω_{sid}). Here, a short river system (i.e., a residence time = 1 kyr) is assumed. According to Postma (1981), $\log_{10}\Omega_{sid}$ increases with an increase in pH: $\log_{10}\Omega_{sid} \sim 1$ at $pH = \sim 7.6$, and $\log_{10}\Omega_{sid} \sim 0$ at $pH = \sim 6.4$ (Fig. 9 of Postma, 1981; see also Fig. C.2). The upper axis represents the corresponding pH, which is derived by fitting the data of Postma (1981) (see also Fig. C.2).

shown in Fig. 4, the upper end of pH is at 7.1 even assuming a siderite supersaturation case (i.e., $\Omega_{sid} = 10$) and decreases if assuming lower Ω_{sid}. Based on the data of Postma (1981), pH < 7.1 corresponds to $\log_{10}\Omega_{sid} < 0.6$ (Fig. C.2). Hence, the constraint of pH_2 would be around 4×10^{-2} bar (Fig. 6), which roughly corresponds to the constraint of pH_2 for the siderite saturation case.

5.4. Effect of river length

The longer the river length (i.e., the residence time in a river) is, the lower the threshold pH_2 (Tables 3 and 4). However, there is not sufficient information available from the locations described in Section 2 to determine exact river length. In general, the Archean landmass size might have been smaller than at present, noting that the continental growth rate has large uncertainties (e.g., Spencer et al., 2017). If the continental size was indeed smaller than present, short river lengths would have been more likely. For a conservative estimate of pH_2, we consider the shortest residence time (1 kyr), which yields an upper limit of pH_2 of $\sim 10^{-2}$ bar or less (Table 2).

5.5. Effect of initial radius

The survival time is defined as the time in which a magnetite particle with an initial radius = 0.25 mm disappears. The survival time depends linearly on the initial radius (see Eq. (16)) especially for a relatively reductive environment ($pH_2 > 10^{-2}$ bar; i.e., the biotic reductive dissolution of magnetite occurs). Hence, if the initial radius is larger than 0.25 mm, the survival time is also larger. For example, assuming the initial radius was 0.5 mm, the survival time would be two times larger than the values shown in Figs. 3 and 5.

The integration of Eq. (9) also indicates that the timescale in which a magnetite particle shrinks linearly depend on the radius change:

$$t = \frac{\Delta R}{v r_{red}}, \tag{20}$$

where ΔR is the difference between initial and final radii of a magnetite particle. Thus, the timescale in which a magnetite radius shrinks from $R = 0.5$ mm to $R = 0.25$ mm is equal to the timescale in which a magnetite radius shrinks from $R = 0.25$ mm to $R = 0$ mm (i.e., the survival time in Eq. (16)).

Therefore, if the radius change is 10 times larger than that of the nominal case (0.25 mm), the survival time and the upper limit of pH_2 are also 10 times larger. On the other hand, if the shrunk radius is 10 times smaller than 0.25 mm, the survival time and the upper limit of pH_2 are also 10 times smaller.

5.6. Effect of maghemite reduction rate

As explained in Section 4 and Appendix B, the survival time depends also on the maghemite reduction rate if $pH_2 <\sim 10^{-2}$ bar. However, considering the plausible range of pCO_2, the survival time is at least larger than thousands of years for $pH_2 <\sim 10^{-2}$ bar. Hence, the maghemite reduction rate does not affect the upper limit on pH_2 for the short river length (i.e., $t_{res} = 1$ kyr), as summarized in Table 5.

On the other hand, for a long river system, the threshold pH_2 (Table 5) tends to be lower than the values summarized in Table 2. However, if maghemite reduction is extremely slow, the threshold pH_2 for a long river system is equal to that for a short river system (Tables 2 and 5). This would mean 4×10^{-2} bar to 8×10^{-2} bar as upper limits on pH_2.

5.7. Constraint under abiotic conditions

The abiotic reductive dissolution rate of magnetite should be lower than the biotic reductive dissolution rate. According to laboratory experiments by Schütz et al. (2015), the concentration of ferrous ions released from microbial reduction of magnetite is roughly 70 times larger

Table 3
Upper limit on pH_2 for the case with 1% Archean atmospheric CH_4. Here, the survival time (t_{surv}) is compared with different residence times (t_{res}). See also Table 2.

	pH_2 [bar]			
	$t_{res} = 1$ kyr	$t_{res} = 10$ kyr	$t_{res} = 100$ kyr	$t_{res} = 500$ kyr
Fresh water	4.6×10^{-2}	5.5×10^{-3}	6.1×10^{-4}	2.9×10^{-4}
Siderite saturation	3.7×10^{-2}	5.5×10^{-3}	5.5×10^{-4}	2.9×10^{-4}
Siderite supersaturation	2.9×10^{-1}	2.9×10^{-1}	2.9×10^{-1}	2.9×10^{-1}

Table 4
Upper limit on pH_2 for the case without Archean atmospheric CH_4. See also Tables 2 and 3.

	pH_2 [bar]			
	$t_{res} = 1$ kyr	$t_{res} = 10$ kyr	$t_{res} = 100$ kyr	$t_{res} = 500$ kyr
Fresh water	7.7×10^{-2}	8.0×10^{-3}	8.1×10^{-4}	1.7×10^{-4}
Siderite saturation	3.2×10^{-2}	4.7×10^{-3}	4.7×10^{-4}	9.4×10^{-5}
Siderite supersaturation	3.8×10^{-2}	2.2×10^{-2}	2.2×10^{-2}	2.2×10^{-2}

Table 5
Upper limit on pH_2 with different assumptions on maghemite reduction. The residence time of a particle in a river is assumed to be 1 kyr. See also Table 2 and Section B.

	pH_2 [bar]	
	Fast	Slow
Short river system (t_{res} = 1 kyr)		
Fresh water	1.3×10^{-2}	4.6×10^{-2}
Siderite saturation	3.7×10^{-2}	3.7×10^{-2}
Siderite supersaturation	2.9×10^{-1}	2.9×10^{-1}
Long river system (t_{res} = 100 kyr)		
Fresh water	2.9×10^{-4}	4.6×10^{-2}
Siderite saturation	2.9×10^{-4}	1.3×10^{-2}
Siderite supersaturation	2.9×10^{-1}	2.9×10^{-1}

than concentration resulted from abiotic reduction of magnetite under pH = 7 even though during the experiment, cell concentration decreased. Accordingly, under pH = 7, the biotic rate (r_{red}) calculated with Eq. (2) is higher by a factor of 70 or more than the abiotic rate. Considering the optimum pH of Fe(III) reducing bacteria (pH 5; Kostka and Nealson, 1995), the difference between biotic and abiotic rates would be much larger under pH = 5 than under pH = 7. On the other hand, abiotic reductive dissolution would monotonically increase with the decrease in pH, which would be different from the pH-dependence of biotic reductive dissolution. Hence, the difference between biotic and abiotic rates might be smaller for lower pH (e.g., pH = 1) than 70. Therefore, we simply treated the rate calculated by Eq. (2) as an upper estimate for the abiotic reductive dissolution rate of magnetite.

If the abiotic magnetite (maghemite) reduction is 10 times slower than the biotic rate assumed here, then, the threshold pH_2 is 10 times higher than the value in Table 2. Thus, if we do not assume Fe(III)-reducing bacteria at 3.0 Ga, detrital magnetite allows several 10^{-1} bar of hydrogen to exist (although there are other reasons, which is discussed below, that makes this unlikely).

5.8. Effect of physical weathering

Physical weathering may decrease the survival time although it is not considered in this study. This effect would decrease the survival time and the threshold pH_2 below which magnetite particles are preserved. Therefore, our estimate of $\sim 10^{-2}$ bar is conservative.

5.9. Comparison with previous works

A constraint of $< 10^{-2}$ bar would preclude H_2 acting as an Archean greenhouse gas (Sagan, 1977; Wordsworth and Pierrehumbert, 2013) and prohibit a strongly reducing Archean atmosphere; however, we cannot say from these Archean data anything about the Hadean atmosphere (Miller, 1953; Miller and Urey, 1959). Notably, the constraint we derive is consistent with the values of pH_2 ($\sim 10^{-4}$ bar) expected from an Archean biosphere that includes methanogens (Wolfe and Fournier, 2018), which consume H_2 and convert it to CH_4 (Kharecha et al., 2005; Ozaki et al., 2018). In addition, in the presence of methanogens, the atmosphere would contains a substantial amount of atmospheric CH_4. Hence, the case with CH_4 is plausible (i.e., the upper limit of $pH_2 = 10^{-2}$ bar).

Zahnle et al. (2019) recently estimated that the total hydrogen expressed in H_2 equivalents (i.e., $H_2 + 2CH_4 + H_2S + \cdots$) in the ~ 3.5 Ga Archean atmosphere must have been $\geqslant 1\%$ (or $\geqslant 0.5\%$ CH_4) to explain the fractionation of xenon isotopes by drag from hydrogen that escapes to space. If our H_2 constraint ($\sim 10^{-2}$ bar) is general for the Archean, it means that most of the hydrogen driving that escape must have been in the form of methane, consistent with previous hypotheses (Catling et al., 2001) and data (Zahnle et al., 2019).

6. CONCLUSIONS

We examined the timescale for the survival of a detrital magnetite particle in an Archean river under various conditions of pH_2 and pCO_2 using a kinetic model. The timescale for a magnetite particle to chemically convert into a soluble state depends mainly on the biotic reductive dissolution rate of magnetite. Thus, the timescale depends mainly on pH_2, not on pCO_2. Consequently, a lower value of pH_2 increases the survival time. If pH_2 is lower than $\sim 10^{-2}$ bar, a magnetite particle with initial radius of 0.25 mm can be preserved for ~ 1 kyr or even longer if microbial reduction occurs.

Previous papers (see Section 2) have reported the existence of detrital magnetite grains in Archean sandstones, and our calculations constrain the pH_2 depending on the residence time of the grains in a river. The existence of detrital magnetite particles indicates that pH_2 in the Archean was below $\sim 10^{-2}$ bar, assuming Fe(III)-reducing microbes and residence times for particles in short river systems (1 kyr; Johnson et al., 2014). Considering long river systems, the threshold pH_2 would be even lower but also depend on the maghemite reduction rate which is unclear.

A constraint of relatively low pH_2 is consistent with pH_2 values expected if the anoxic biosphere at the time included methanogens (Kharecha et al., 2005; Ozaki et al., 2018), as indicated by phylogenetic studies (Wolfe and Fournier, 2018) and isotopic data (Ueno et al., 2006; Stüeken et al., 2017; Stüeken and Buick, 2018).

ACKNOWLEDGMENTS

We thank Roger Buick for important discussions of Archean geology. We are grateful to Joshua Krissansen-Totton and Jonathan Toner for their useful comments. Two anonymous reviewers and the Executive Editor (Jeffrey G. Catalano), in particular, provided very important comments. This work was supported by a grant from the Simons Foundation (SCOL award 511570 to DCC).

APPENDIX A. PH-DEPENDENCE OF BIOTIC REDUCTIVE DISSOLUTION OF MAGNETITE

As shown in Kostka and Nealson (1995), biotic reductive dissolution of magnetite depends on pH, and the pH

dependence is neither linear nor monotonic. In this study, we modeled the pH dependence by fitting the results of Kostka and Nealson (1995) (Fig. A.1).

APPENDIX B. SENSITIVITY TEST FOR MAGHEMITE REDUCTION

Under a less reductive environment, ferrous ion dissolves from magnetite before magnetite is reduced, and maghemite is formed (White et al., 1994). Then, maghemite would be reduced and dissolved, but the rate of such a reaction is unclear. For a nominal case, we assume that the Fe^{2+} release rate via biotic reduction of maghemite is equal to that of the biotic reductive dissolution of magnetite motivated by the structural similarity of magnetite and maghemite (Eq. (8)). Additionally, we consider two extreme cases for the maghemite reduction rate.

For one end-member case, we assume that the maghemite reduction is extremely fast. Under such a condition, a maghemite layer cannot be formed, so, a magnetite particle always contacts with surrounding water as shown in Fig. 1b. Hence, the survival time is controlled by the acid dissolution rate of magnetite (r_{diss} in Eq. (5)) as follows:

$$t_{diss} = \frac{R_0}{v r_{diss}}, \tag{B.1}$$

where R_0 is an initial radius of a magnetite particle, and v is the molar volume of magnetite. Hereafter, the survival time for this case is named as a "dissolution time". As shown in Eq. (5), the dissolution time depends only on pH, which is also shown by the vertical line in the region below a dashed gray line in Fig. B.1a.

For another end-member case, we assume that the maghemite reduction is extremely slow. Under such a condition, maghemite cannot dissolve, so, the radius of a maghemite layer is constant at R_0. Hence, the survival time is controlled by the acid dissolution rate of magnetite limited by the supply of hydrogen ions (r_{diff} in Eq. (6)). The survival time is the diffusion time (Eq. (17)) and depends only on pH, which is also shown by the vertical contour lines in the region below a dashed gray line in Fig. B.1b.

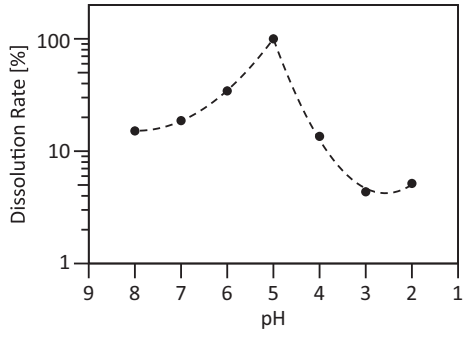

Fig. A.1. Dependence of biotic reductive dissolution rate on pH relative to the rate for pH 5. Black-filled circles corresponds to the results shown in Fig. 2c of Kostka and Nealson (1995). And dashed lines represent the fitting function used in this study.

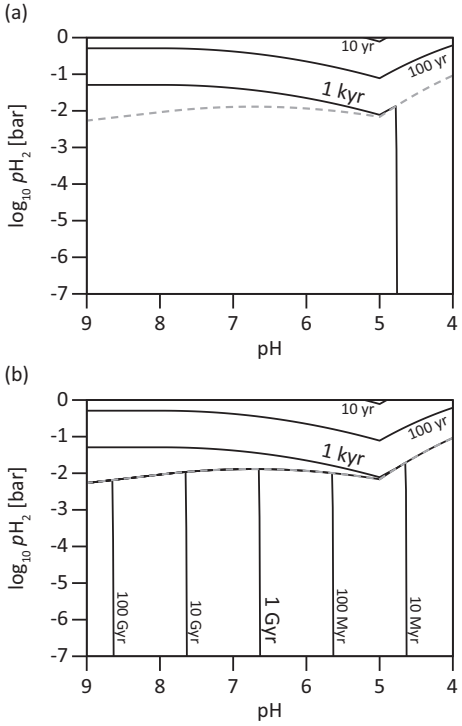

Fig. B.1. Biotic survival time as a function of pH and pH_2. The dashed gray line represents the pH_2 at which biotic reductive dissolution rate for magnetite is equal to acid dissolution rate of magnetite. When pH_2 is higher than this line, biotic reductive dissolution of magnetite occurs; otherwise, acid dissolution of magnetite occurs. For (a), it is assumed that magnetite is always in contact with surrounding water (Fig. 1b) as an end member case for fast maghemite reduction. For (b), it is assumed that a radius of maghemite layer does not change when maghemite is formed (Fig. 1c) as an end member case for slow maghemite reduction.

As shown in Fig. B.1, the survival time strongly depends on the maghemite reduction rate for a less reductive environment. However, considering the pH range plausible for Archean river water (pH > 5; see also Fig. 4), the survival time is at least longer than one thousand years.

APPENDIX C. OTHER SUPPLEMENTARY MATERIALS

Upper limits on pH_2 for different assumption are summarized in Tables 3-5. Table 3 shows the limit of a case with 1% Archean atmospheric CH_4. Table 4 shows the limit of a case without Archean atmospheric CH_4. Table 5 shows the limit assuming different maghemite reduction rates: for the fast case, maghemite is immediately reduced and dissolved into solution (i.e., there is no maghemite layer), on the other hand, for the slow case, maghemite is not reduced (i.e., the radius of maghemite layer does not change). See also Appendix B.

Fig. C.1 shows cumulative dissolution of pCO_2 following Krissansen-Totton et al. (2018). Fig. C.2 shows a saturation state at which siderite precipitates (Ω_{sid}) as a function of pH according to Postma (1981).

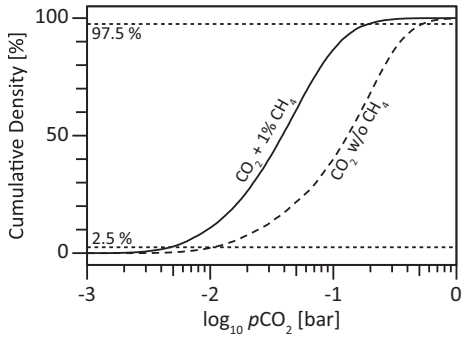

Fig. C.1. Cumulative density of partial pressure of atmospheric CO_2 (pCO_2) at 3.0 Ga. Solid line represent the case where 1% of atmospheric methane is assumed. On the other hand, the dashed line represents the case without atmospheric methane. The distributions of pCO_2 are calculated following Krissansen-Totton et al. (2018). Hence, the distribution for the case without methane (the dashed line) corresponds to the results shown in Fig. 3B of Krissansen-Totton et al. (2018). Similarly, the distribution for the case with 1% CH_4 (the black solid line) corresponds to the results shown in Fig. 5B of Krissansen-Totton et al. (2018).

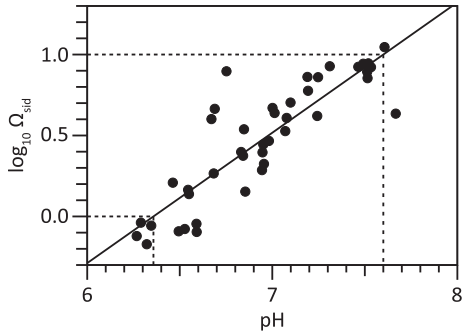

Fig. C.2. Saturation state of siderite at which siderite precipitates (Ω_{sid}) as a function of pH. Black-filled circles are the data compiled in Postma (1981). Solid black line is the fitting function for black-filled circles ($\log_{10}\Omega_{sid} = 0.805 \times pH - 5.12$).

REFERENCES

Arora, M. (1991). Geology, geochemistry and tectonic setting of conglomerates and quartzites of the Bababudan schist belt Karnataka nucleus, India. PhD thesis.

Catling D. C., Zahnle K. J. and McKay C. P. (2001) Biogenic methane, hydrogen escape, and the irreversible oxidation of early Earth. *Science* **293**(5531), 839–843. https://doi.org/10.1126/science.1061976.

Cornell R. M. and Schwertmann U. (2003) *The Iron Oxides: Structure, Properties, Reactions, Occurrences and Uses*. John Wiley Sons. https://doi.org/10.1002/3527602097.

Craddock P. R. and Dauphas N. (2011) Iron and carbon isotope evidence for microbial iron respiration throughout the Archean. *Earth Planet. Sci. Lett.* **303**(1–2), 121–132. https://doi.org/10.1016/j.epsl.2010.12.045.

Czaja A. D., Johnson C. M., Beard B. L., Roden E. E., Li W. Q. and Moorbath S. (2013) Biological Fe oxidation controlled deposition of banded iron formation in the ca. 3770 Ma Isua supracrustal belt (west Greenland). *Earth Planet. Sci. Lett.* **363**, 192–203. https://doi.org/10.1016/j.epsl.2012.12.025.

Donaldson J. A. and de Kemp E. A. (1998) Archaean quartz arenites in the canadian shield: examples from the Superior and Churchill provinces. *Sed. Geol.* **120**(1–4), 153–176. https://doi.org/10.1016/S0037-0738(98)00031-1.

Driese S. G., Jirsa M. A., Ren M. H., Brantley S. L., Sheldon N. D., Parker D. and Schmitz M. (2011) Neoarchean paleoweathering of tonalite and metabasalt: implications for reconstructions of 2.69 Ga early terrestrial ecosystems and paleoatmospheric chemistry. *Precambr. Res.* **189**(1–2), 1–17. https://doi.org/10.1016/j.precamres.2011.04.003.

Gough D. O. (1981) Solar interior structure and luminosity variations. *Sol. Phys.* **74**(1), 21–34. https://doi.org/10.1007/BF00151270.

Haqq-Misra J. D., Domagal-Goldman S. D., Kasting P. J. and Kasting J. F. (2008) A revised, hazy methane greenhouse for the Archean Earth. *Astrobiology* **8**(6), 1127–1137. https://doi.org/10.1089/ast.2007.0197.

Hoehler T. M., Albert D. B., Alperin M. J., Bebout B. M., Martens C. S. and Des Marais D. J. (2002) Comparative ecology of H_2 cycling in sedimentary and phototrophic ecosystems. *Antonie Van Leeuwenhoek* **81**(1–4), 575–585. https://doi.org/10.1023/A:1020517924466.

Iben I. (1967) Stellar evolution within and off main sequence. *Ann. Rev. Astron. Astrophys.* **5**, 571–626. https://doi.org/10.1146/annurev.aa.05.090167.003035.

Jackson B. E. and McInerney M. J. (2002) Anaerobic microbial metabolism can proceed close to thermodynamic limits. *Nature* **415**(6870), 454–456.

Johnson C. M., Beard B. L. and Roden E. E. (2008) The iron isotope fingerprints of redox and biogeochemical cycling in the modern and ancient Earth. *Annu. Rev. Earth Planet. Sci.* **36**, 457–493. https://doi.org/10.1146/annurev.earth.36.031207.124139.

Johnson J. E., Gerpheide A., Lamb M. P. and Fischer W. W. (2014) O_2 constraints from paleoproterozoic detrital pyrite and uraninite. *Geol. Soc. Am. Bull.* **126**(5–6), 813–830. https://doi.org/10.1130/B30949.1.

Kanzaki Y. and Murakami T. (2015) Estimates of atmospheric CO_2 in the Neoarchean-Paleoproterozoic from paleosols. *Geochimica Et Cosmochimica Acta* **159**, 190–219. https://doi.org/10.1016/j.gca.2015.03.011.

Kharecha P., Kasting J. and Siefert J. (2005) A coupled atmosphere-ecosystem model of the early Archean Earth. *Geobiology* **3**(2), 53–76. https://doi.org/10.1111/j.1472-4669.2005.00049.x.

Kostka J. E. and Nealson K. H. (1995) Dissolution and reduction of magnetite by bacteria. *Environ. Sci. Technol.* **29**(10), 2535–2540. https://doi.org/10.1021/es00010a012.

Krissansen-Totton J., Arney G. N. and Catling D. C. (2018) Constraining the climate and ocean pH of the early Earth with a geological carbon cycle model. *Proc. Natl. Acad. Sci. USA* **115**(16), 4105–4110. https://doi.org/10.1073/pnas.1721296115.

Kuramoto K., Umemoto T. and Ishiwatari M. (2013) Effective hydrodynamic hydrogen escape from an early Earth atmosphere inferred from high-accuracy numerical simulation. *Earth Planet. Sci. Lett.* **375**, 312–318. https://doi.org/10.1016/j.epsl.2013.05.050.

Miller S. L. (1953) A production of amino acids under possible primitive Earth conditions. *Science* **117**(3046), 528–529. https://doi.org/10.1126/science.117.3046.528.

Miller S. L. and Urey H. C. (1959) Organic compound synthesis on the primitive Earth. *Science* **130**(3370), 245–251. https://doi.org/10.1126/science.130.3370.245.

Ozaki K., Tajika E., Hong P. K., Nakagawa Y. and Reinhard C. T. (2018) Effects of primitive photosynthesis on Earth's early climate system. *Nat. Geosci.* **11**(1), 55. https://doi.org/10.1038/s41561-017-0031-2.

Pavlov A. A., Brown L. L. and Kasting J. F. (2001) UV shielding of NH_3 and O_2 by organic hazes in the Archean atmosphere. *J. Geophys. Res.-Planets* **106**(E10), 23267–23287. https://doi.org/10.1029/2000JE001448.

Postma D. (1981) Formation of siderite and vivianite and the pore-water composition of a recent bog sediment in denmark. *Chem. Geol.* **31**(3), 225–244. https://doi.org/10.1016/0009-2541(80)90088-1.

Ramirez R. M., Kopparapu R., Zugger M. E., Robinson T. D., Freedman R. and Kasting J. F. (2014) Warming early mars with CO_2 and H_2. *Nat. Geosci.* **7**(1), 59–63. https://doi.org/10.1038/Ngeo2000.

Rye R., Kuo P. H. and Holland H. D. (1995) Atmospheric carbon-dioxide concentrations before 2.2-billion years ago. *Nature* **378**(6557), 603–605. https://doi.org/10.1038/378603a0.

Sagan C. (1977) Reducing greenhouses and temperature history of Earth and Mars. *Nature* **269**(5625), 224–226. https://doi.org/10.1038/269224a0.

Schink B. (1997) Energetics of syntrophic cooperation in methanogenic degradation. *Microbiol. Mol. Biol. Rev.* **61**(2), 262–280, doi:Journal Article.

Schütz M. K., Bildstein O., Schlegel M. L. and Libert M. (2015) Biotic Fe(III) reduction of magnetite coupled to H_2 oxidation: implication for radioactive waste geological disposal. *Chem. Geol.* **419**, 67–74. https://doi.org/10.1016/j.chemgeo.2015.10.039.

Sekiya M., Nakazawa K. and Hayashi C. (1980) Dissipation of the primordial terrestrial atmosphere due to irradiation of the solar euv. *Prog. Theoret. Phys.* **64**(6), 1968–1985. https://doi.org/10.1143/PTP.64.1968.

Spencer C. J., Roberts N. M. W. and Santosh M. (2017) Growth, destruction, and preservation of Earth's continental crust. *Earth Sci. Rev.* **172**, 87–106. https://doi.org/10.1016/j.earscirev.2017.07.013.

Srinivasan R. and Ojakangas R. W. (1986) Sedimentology of quartz-pebble conglomerates and quartzites of the Archean Bababudan group, Dharwar craton, South-India – evidence for early crustal stability. *J. Geol.* **94**(2), 199–214 <http://www.jstor.org/stable/30062146>.

Stüeken E. E. and Buick R. (2018) Environmental control on microbial diversification and methane production in the Mesoarchean. *Precambr. Res.* **304**, 64–72. https://doi.org/10.1016/j.precamres.2017.11.003.

Stüeken E. E., Buick R., Anderson R. E., Baross J. A., Planavsky N. J. and Lyons T. W. (2017) Environmental niches and metabolic diversity in neoarchean lakes. *Geobiology* **15**(6), 767–783. https://doi.org/10.1111/gbi.12251.

Sweeton F. H. and Baes, Jr., C. F. (1970) The solubility of magnetite and hydrolysis of ferrous ion in aqueous solutions at elevated temperatures. *J. Chem. Thermodyn.* **2**(4), 479–500. https://doi.org/10.1016/0021-9614(70)90098-4.

Tian F., Toon O. B., Pavlov A. A. and De Sterck H. (2005) A hydrogen-rich early Earth atmosphere. *Science* **308**(5724), 1014–1017. https://doi.org/10.1126/science.1106983.

Tosca N. J., Ahmed I. A. M., Tutolo B. M., Ashpitel A. and Hurowitz J. A. (2018) Magnetite authigenesis and the warming of early mars. *Nat. Geosci.* **11**(9), 635–639. https://doi.org/10.1038/s41561-018-0203-8.

Trendall A. F., deLaeter J. R., Nelson D. R. and Mukhopadhyay D. (1997) A precise zircon U-Pb age for the base of the BIF of the Mulaingiri formation, (Bababudan group, Dharwar supergroup) of the Karnataka craton. *J. Geol. Soc. India* **50**(2), 161–170, doi: Journal Article.

Ueno Y., Yamada K., Yoshida N., Maruyama S. and Isozaki Y. (2006) Evidence from fluid inclusions for microbial methanogenesis in the early Archaean era. *Nature* **440**(7083), 516–519. https://doi.org/10.1038/nature04584.

Vargas M., Kashefi K., Blunt-Harris E. L. and Lovley D. R. (1998) Microbiological evidence for Fe(III) reduction on early Earth. *Nature* **395**(6697), 65–67. https://doi.org/10.1038/25720.

Wen C. Y. (1968) Noncatalytic heterogeneous solid fluid reaction models. *Ind. Eng. Chem.* **60**(9), 34–54. https://doi.org/10.1021/ie50705a007.

White A. F., Peterson M. L. and Hochella M. F. (1994) Electrochemistry and dissolution kinetics of magnetite and ilmenite. *Geochimica Et Cosmochimica Acta* **58**(8), 1859–1875. https://doi.org/10.1016/0016-7037(94)90420-0.

Wolfe J. M. and Fournier G. P. (2018) Horizontal gene transfer constrains the timing of methanogen evolution. *Nat. Ecol. Evol.* **2**(5), 897–903. https://doi.org/10.1038/s41559-018-0513-7.

Wordsworth R. and Pierrehumbert R. (2013) Hydrogen-nitrogen greenhouse warming in Earth's early atmosphere. *Science* **339**(6115), 64–67. https://doi.org/10.1126/science.1225759.

Zahnle K., Claire M. and Catling D. (2006) The loss of mass-independent fractionation in sulfur due to a palaeoproterozoic collapse of atmospheric methane. *Geobiology* **4**(4), 271–283. https://doi.org/10.1111/j.1472-4669.2006.00085.x.

Zahnle K. J., Gacesa M. and Catling D. C. (2019) Strange messenger: a new history of hydrogen on Earth, as told by xenon. *Geochimica Et Cosmochimica Acta* **244**, 56–85. https://doi.org/10.1016/j.gca.2018.09.017.

Associate editor: Rajdeep Dasgupta